SCIENTIFIC REPORTS

OPEN

SUBJECT AREAS:
TRANSMISSION ELECTRON MICROSCOPY
GRAPHENE
NANOSCALE MATERIALS

Received
13 May 2014

Accepted
20 August 2014

Published
6 October 2014

Correspondence and requests for materials should be addressed to S.J.H. (sarah.haigh@manchester.ac.uk) or J.A.H. (j.a.hinks@hud.ac.uk)

* Current address: Department of Physics and Energy, University of Limerick, Limerick, Ireland.

In-situ observation and atomic resolution imaging of the ion irradiation induced amorphisation of graphene

C.-T. Pan[1,2], J. A. Hinks[3], Q. M. Ramasse[4], G. Greaves[3], U. Bangert[1]*, S. E. Donnelly[3] & S. J. Haigh[1]

[1]School of Materials, University of Manchester, Material Science Centre, Grosvenor Street, Manchester, M13 9PL, United Kingdom, [2]School of Physics and Astronomy, University of Manchester, Manchester, Oxford Road, M13 9PL, United Kingdom, [3]School of Computing and Engineering, University of Huddersfield, HD1 3DH, United Kingdom, [4]SuperSTEM Laboratory, STFC Daresbury Campus, Keckwick Lane, Daresbury WA4 4AD, United Kingdom.

Ion irradiation has been observed to induce a macroscopic flattening and in-plane shrinkage of graphene sheets without a complete loss of crystallinity. Electron diffraction studies performed during simultaneous *in-situ* ion irradiation have allowed identification of the fluence at which the graphene sheet loses long-range order. This approach has facilitated complementary *ex-situ* investigations, allowing the first atomic resolution scanning transmission electron microscopy images of ion-irradiation induced graphene defect structures together with quantitative analysis of defect densities using Raman spectroscopy.

The engineering of the physical and electronic properties of two dimensional materials requires control over sheet conformation as well as atomic scale lattice defects[1–6]. For example, there is often a reduction in carrier mobility for defective graphene material[2] and introducing point defects by ion irradiation can induce spin-half paramagnetism[6]. It is clear that for the remarkable properties of graphene to be effectively harnessed, the nature and extent of defects must be carefully controlled. Correlating physical property variations with ion-induced structural changes requires direct characterisation of defect structures. Transmission electron microscope (TEM) imaging provides a powerful means of observing both types of structural feature. Macroscopic bending produces characteristic bend contours in conventional bright-field (BF) images while aberration-corrected TEM and scanning transmission electron microscopy (STEM) are almost unparalleled in their capabilities for achieving atomic resolution in the imaging of defective free-standing graphene[7–16]. Coupled with electron energy loss spectroscopy (EELS), STEM can provide information on local bonding environments[17–19] and the presence of individual atomic impurities[20–24]. To date, the majority of (S)TEM studies of defective graphene have relied on defects induced either during the growth process[5,8,15] or by imaging with high energy electrons[7,16,25,26] with only a few recent papers reporting high-resolution TEM imaging of ion irradiated graphene[12–14]. In this paper we demonstrate that ion irradiation could provide a simple means for ironing out macroscopic corrugations in suspended graphene sheets. In addition, we report the first atomic resolution imaging of defect structures produced in single-layer graphene using ion irradiation with the corresponding average defect densities evaluated via Raman spectroscopy.

Results

Ironing out macroscopic corrugations in suspended graphene sheets. The low magnification bright field TEM images in Figs. 1a(i) and 1b(i) show the macroscopic morphology of a few-layer graphene sheet suspended on a Quantifoil TEM grid before a(i) and after b(i) ion irradiation with 30 keV He ions to a fluence of 8.0×10^{14} ions cm^{-2}. A sample thickness of ~10 graphene layers was estimated from the optical image contrast of the flake on a SiO_2/Si substrate before it was transferred to the Quantifoil TEM grid[27]. Fig. 1a(i) shows bend contours[28] due to the presence of macroscopic wrinkles/corrugations in the suspended graphene before irradiation. During ion irradiation the bend contours are observed to gradually disappear until at a fluence of 8.0×10^{14} ions cm^{-2} they are completely removed suggesting a flattening of the graphene sheets (Fig. 1b(i)). Similar loss of bend contours has been observed for thicker samples irradiated with 30 keV He ions and for few layer graphene irradiated with 6 keV Ar ions (further details in supplementary materials Figs. S1 and S2).

The loss of bend contours in the graphene sheets as a result of modest ion irradiation could be produced from a significant loss of crystallinity in the graphene sheets. To investigate this possibility, we have recorded comple-

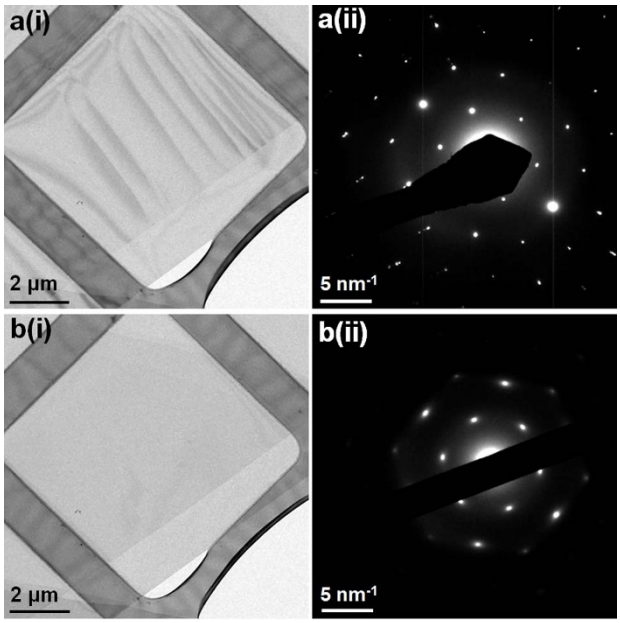

Figure 1 | Low-magnification bright-field (BF) TEM imaging and electron diffraction for suspended few-layer graphene sheets (a) before and (b) after in-situ ion irradiation with 30 keV He ions to a fluence of 8.0×10^{14} ions cm^{-2}. Complementary *in-situ* selected area electron diffraction patterns acquired before irradiation (a(ii)) and after irradiation (b(ii)) are displayed to the right of the BF TEM images. These were acquired under identical diffraction conditions and are both displayed with the same intensity scale.

mentary diffraction patterns during *in-situ* ion irradiation for both single-layer (Fig. 2) and few-layer graphene samples (Figs. 1a(ii), 1b(ii) and S2). A complete loss of bend contours is observed after He ion fluences of $\sim 10^{15}$ ions cm^{-2} at which fluence the graphene is still highly crystalline as demonstrated by the sharp peaks in the diffraction pattern in Fig. 1b(ii). Figure 2 shows example images from a continuous series of diffraction patterns acquired as a function of ion irradiation fluence illustrating the effect on the crystallinity. We find that diffraction patterns for irradiated single layer graphene are still highly crystalline and nearly indistinguishable from those obtained for pristine graphene – even for much larger He ion fluences up to 3.0×10^{15} ions cm^{-2} (Fig. 2c). This reveals that a loss of crystallinity is not likely to be responsible for the disappearance of bend contours illustrated in Fig. 1. Instead we conclude that the observed reduction in bend contours is a result of 'ironing out' the macroscopic corrugations of the free-standing sheets – a phenomenon that occurs, at least in part, due to gradual irradiation-induced in-plane contraction of the graphene[29] which is pinned at the edges by van der Waals attraction to the Quantifoil support grid. Irradiation-induced in-plane shrinkage of the graphene sheet will therefore produce an in-plane tension that favours a flattening of the suspended graphene region (see Fig. S1). Irradiation induced in-plane shrinkage is well known for bulk graphite, although the atomistic mechanism for this behaviour is still the subject of considerable debate[30–32]. Previous work on graphite has shown that the lattice shrinkage scales with the level of ion irradiation and can induce a wide variety of structural defects where a non-uniform damage profile exists in the material[33]. *Stopping and Range of Ions in Matter* (SRIM) Monte Carlo calculations[33,34] for 30 keV He ions and a graphene thicknesses of up to 10 nm, demonstrate that for few-layer graphene the damage profile is effectively constant and thus increased ion fluence is expected to produce uniform contraction in the a/b-directions.

Fig. 2 illustrates the changes in the selected area diffraction pattern recorded *in-situ* using constant illumination conditions for single-layer graphene as a function of 30 keV He ion irradiation up to a fluence of 1.2×10^{16} ions cm^{-2}. Analysis of the diffraction peak intensities in Fig. 2b confirm this is single-layer graphene. For fluences below 3.0×10^{15} ions cm^{-2} (Fig. 2c), the recorded diffraction patterns are nearly indistinguishable from that obtained for the same area of pristine graphene prior to irradiation (Fig. 2b). This suggests that if defects are introduced during this stage they either annihilate quickly or introduce only minor lattice strain. At a greater ion fluence (6.0×10^{15} ions cm^{-2}), the outermost diffraction spots started to show streaking perpendicular to the reciprocal lattice vector, in the directions indicated by the white arrows in Fig. 2d. This demonstrates that ion-irradiation induced defects have introduced distortion into the crystal structure. The streaking of the outer diffraction spots can be observed by comparing the decay in the diffraction intensity parallel and perpendicular to the reciprocal lattice vector for the (1–210) reflection (Figs. 2j and 2k); the full-width half-maximum of the diffraction peak decreases more slowly perpendicular to the reciprocal lattice vector than parallel to it. At a fluence of 9.6×10^{15} ions cm^{-2}, the inner diffraction spots corresponding to the {0-110} lattice reflections also show streaking (Fig. 2e). As irradiation continues the intensity of all the crystalline reflections is gradually reduced (Figs. 2i–k) being replaced by diffuse rings characteristic of amorphous material (Fig. 2d–g). A complete loss of long-range order within the basal planes is observed in the diffraction pattern obtained for a few-layer graphene sample after a higher irradiation fluence (see supplementary information Fig. S2). Similar streaking of diffraction spots is observed for graphene scroll defects and carbon nanotubes[35,36] but in these cases the streaking is only in one direction (perpendicular to the long axis of the tube), whereas we observe a more isotropic streaking of all equivalent crystallographic lattice reflections.

Evolution of the Raman spectra for irradiated graphene. Raman spectroscopy is complementary to TEM imaging and diffraction, ideally suited to obtaining lower spatial resolution information concerning the number of graphene layers and identifying the presence of defects[37–44]. In order to quantify the defect density induced in our single-layer graphene samples, Raman spectroscopy was performed before and after irradiation to different ion fluences (Fig. 3a). The Raman spectra before irradiation exhibit a behaviour typical of suspended single-layer graphene with one sharp double resonant peak (2D peak) and a first-order Raman peak (G peak) with the intensity of latter being significantly lower than that of the former[38]. The absence of a prominent D peak in our graphene samples before ion irradiation suggests that the material is largely defect free, as this peak is known to be activated by the presence of defects in the material[37]. This absence of defects in the pristine samples is in agreement with our TEM and STEM observations of the unirradiated material. The G peak frequency observed for the graphene sample before irradiation was ~ 1580 cm^{-1} suggesting no significant doping in the sample[37,44]. As shown in Fig. 3a, increasing ion irradiation produced additional D, D′ and D + D′ peaks in the Raman spectra, the presence of which is known to be associated with defects in graphene[38,40].

Lucchese *et al.* have proposed a model to aid the interpretation of Raman spectra obtained from defective graphene (Fig. 3b)[39]. They proposed that activation of the D peak requires not only defective graphene (indicated by the red circles in Fig. 3b) but also a surrounding region of crystalline graphene (indicated by the green areas in Fig. 3b). The intensity of the D peak is proportional to the total area of crystalline graphene that is locally-activated by the defects and not to the area of the defective regions themselves. Therefore, when the average defect distance (L_D) is greater than twice the radius of the activated crystalline regions surrounding each defect (R_A), the intensity ratio of the D peak to G peak (I(D)/I(G)) increases in direct proportion to the increasing number of defects (Fig. 3b(i)). However, if the defect density becomes sufficiently high that neighbouring

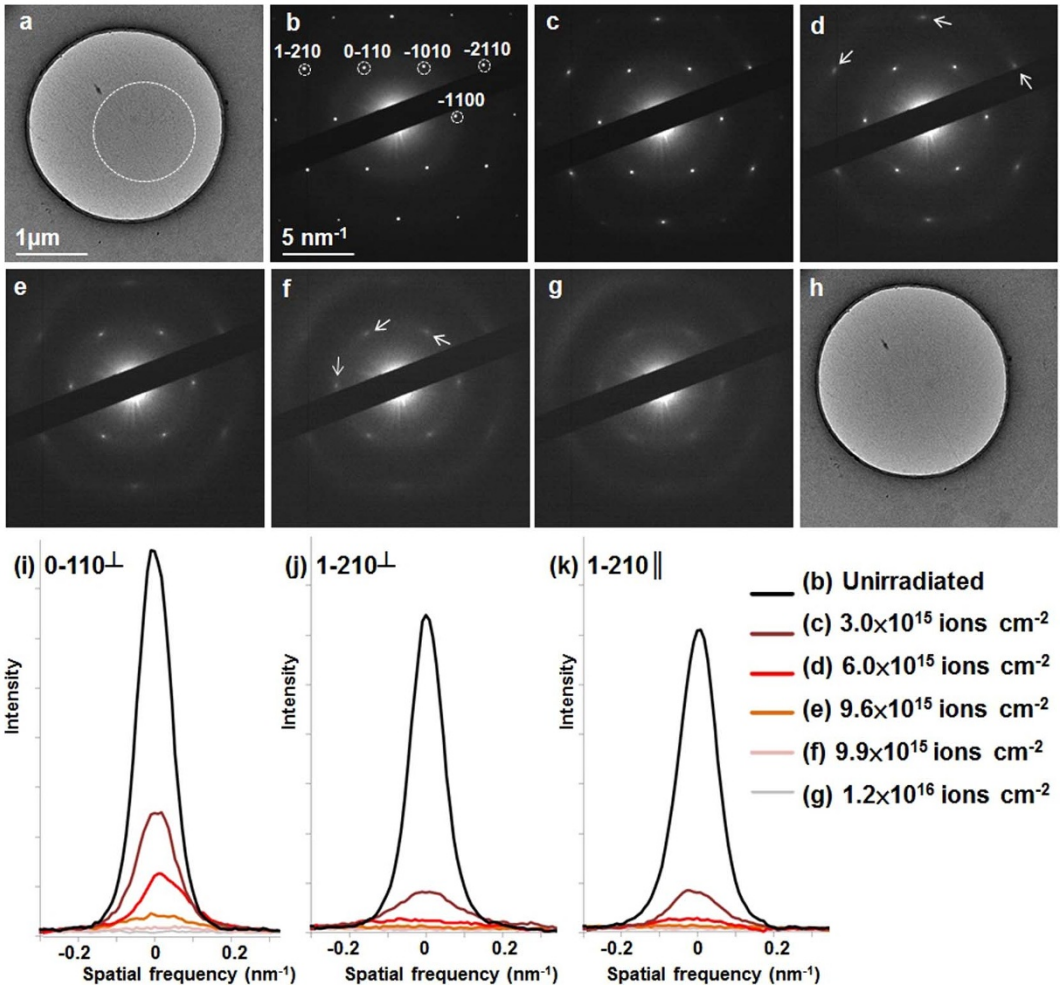

Figure 2 | Electron diffraction patterns recorded *in-situ* for single-layer graphene as a function of 30 keV He ion irradiation. (a) BF TEM image and (b) electron diffraction pattern for the single-layer graphene sheet before ion irradiation. (c)–(g) Show a sequence of selected area electron diffraction patterns acquired during *in-situ* irradiation of the single-layer graphene sheet with 30 keV He ions after fluences of (c) 3.0×10^{15} ions cm^{-2}, (d) 6.0×10^{15} ions cm^{-2}, (e) 9.6×10^{15} ions cm^{-2}, (f) 9.9×10^{15} ions cm^{-2} and (g) 1.2×10^{16} ions cm^{-2}. Selected area region used to acquire diffraction data (b)–(g) is indicated by the dashed circle in (a). (h) BF TEM image after 1.2×10^{16} ions cm^{-2} of irradiation. (i)–(k) Show the reduction in diffraction peak intensity as a function of irradiation dose for a line scan taken: (i) through (0–110) perpendicular to the reciprocal lattice vector; (j) through (1–210) perpendicular to the reciprocal lattice vector; and (k) through (1–210) parallel to the reciprocal lattice vector.

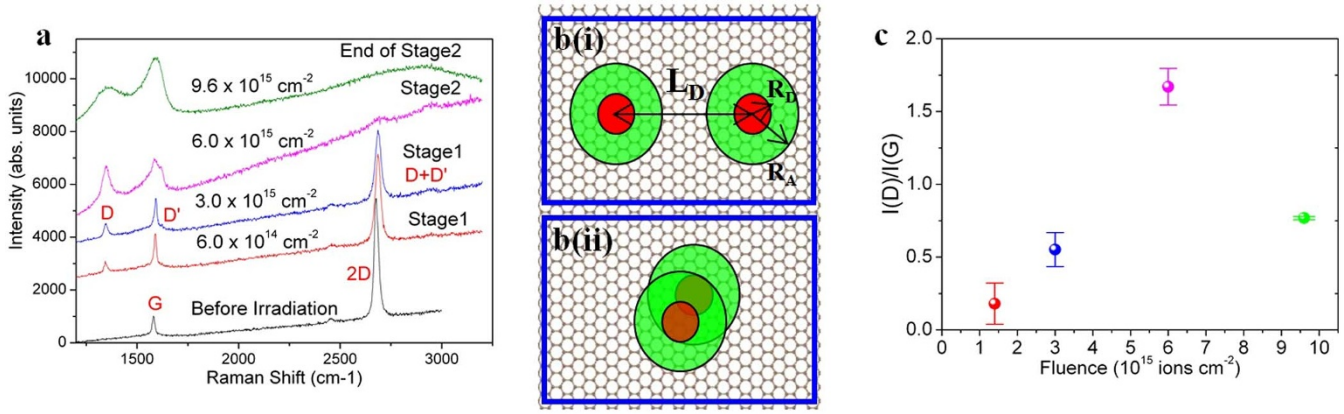

Figure 3 | The evolution of Raman spectra of irradiated single-layer graphene. (a) Raman spectra of single-layer graphene after irradiation with 30 keV He ions at the fluences labelled. (b) Schematic showing situations with b(i) low defect-density ($L_D > 2R_A$) and b(ii) high defect-density ($L_D < 2R_A$)[39]. D peak activated regions (perfect graphene) are indicated by the green areas and D peak inactive regions (defective graphene) are indicated by the red circles[39]. (c) I(D)/I(G) as a function of ion fluence. The fitting method used to calculate the intensity ratio (I(D)/I(G)) is outlined in the supplementary information (Fig. S3).

activated regions begin to overlap (Fig. 3b(ii)), the ratio of I(D)/I(G) decreases with increasing defect density. As shown in Fig. 3c, our samples followed the expected amorphisation trajectory[39] in that I(D)/I(G) initially increased and then decreased for fluences greater than 9.6×10^{15} ions cm^{-2}. Ferrari *et al.*[37] have interpreted the amorphisation trajectory of carbon materials as being described by three stages with the fraction of sp^3 bonds increasing from stage 1 to stage 3. Comparing their results to our measurements (Fig. 3c), we assign the Raman spectra of irradiated graphene shown in Fig. 3a to various stages of the amorphisation process. In particular, a fluence of 6.0×10^{15} ions cm^{-2} is consistent with the start of stage 2 where the bonding begins to change from sp^2 to sp^3 configurations[37]. The result is in good agreement with the evolution of the diffraction patterns in Fig. 2, as any significant sp^3 bonding will produce nanoscale buckling which will in turn lead to streaking of the diffraction spots as observed in Fig. 2d–g to occur at a similar fluence of $\sim 10^{15}$ ions cm^{-2}.

We have estimated the average defect density, σ, assuming $\sigma = 1/L_D^2$ and using the method described in Ref. 39. As summarized in supplementary Table S1, the values of σ for our samples are typically 2–3 orders of magnitude lower than the total ion fluence which is in good agreement with the theoretical predictions of molecular dynamics simulations[3,4]. The simulations suggest that only ~1/100th of incident ions will interact with single-layer graphene under these irradiation conditions[3,4]. The Raman spectra obtained from ion-irradiated graphene were found to be stable for several weeks at room temperature. However, after annealing at 100°C in vacuum for 5 hours we have found that the intensity ratio I(D)/I(G) decreased from 1.06 to 0.42 (supplementary Fig. S4). According to the quantification method in Ref. 39 this change corresponds to an increase in L_D from 12 nm to 20 nm. This behaviour is similar to the hysteresis cycle described by Ferrari *et al*[37] which suggests some defects were removed after annealing - although we cannot rule out the possibility that this result is associated with changes of the surface contamination.

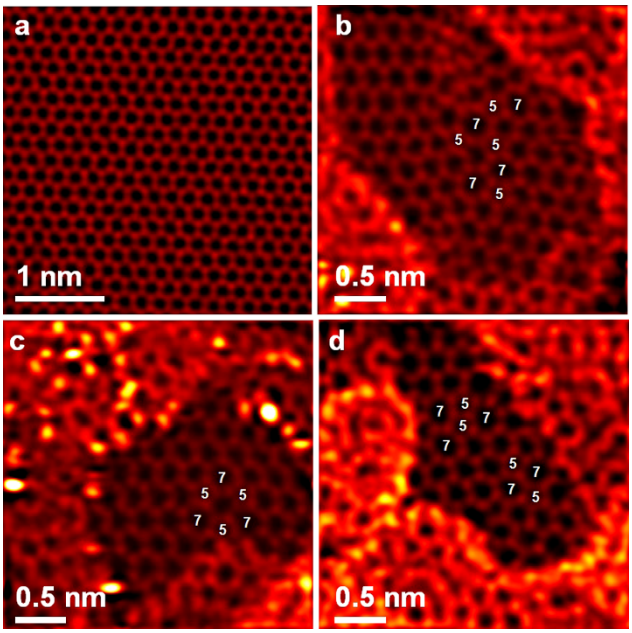

Figure 4 | Atomic resolution HAADF images of single-layer irradiated graphene. (a)–(d) Filtered atomic resolution HAADF images of single-layer irradiated graphene (30 keV He ions) at fluences of (a) 3.0×10^{15} ions cm^{-2} and (b)–(d) 9.6×10^{15} ions cm^{-2}. Bright spots in (c) are heavy atom contaminants (most likely silicon or metal atoms). Pentagon-heptagon (5–7) pairs, a unit cell of the haeckelite structure, Stone-Thrower-Wales defects and Inverse-Stone-Thrower-Wales defects are observed in (b), (c) and (d), respectively. Images have been filtered based on the method as reported in Ref. 48 to improve clarity (raw images are given in supplementary material Fig. S5).

Atomic resolution images of irradiated graphene. To better understand the amorphisation process and the character of the defects induced during ion irradiation, we have performed high-resolution high angle annular dark field (HAADF) STEM imaging of our irradiated samples at different ion fluences (Figs. 4–6). In all cases, the electron beam exposure prior to high-resolution image acquisition was minimized to reduce the possibility of electron-beam induced structural changes. The D peak observed in the Raman spectra for a fluence of 3.0×10^{15} ions cm^{-2} (Fig. 3a) suggests that defects are present at this fluence. However, despite extensive time spent imaging single-layer graphene samples irradiated with fluences of up to 3.0×10^{15} ions cm^{-2} no structural defects were observed in these samples (Fig. 4a). Therefore the presence of the D peak in the corresponding Raman spectra may be simply a result of the presence of adatom-type defects associated with surface contamination[40] or it could be that surface contamination obscured defective regions such that they could not be observed in the STEM. The different spatial resolution of the two techniques makes it difficult to draw firmer conclusions. At a slightly higher fluence of 6.0×10^{15} ions cm^{-2}, corresponding to the onset of streaking in the electron diffraction data, a limited number of structural defects were observed. Only when imaging samples that had been irradiated to a fluence of $\sim 10^{16}$ ions cm^{-2} were structural defects consistently detected in the majority of regions that were sufficiently free from surface contamination to facilitate their clear observation using HAADF STEM (Fig. 4b–d). The observed defects consisted of multiple pentagon-heptagon (5–7) pairs which are known to be produced during structural relaxation after vacancy formation[29]. This type of vacancy creation followed by structural relaxation represents a loss of material from the two dimensional lattice, and an in-plane shrinkage will therefore be required in order to prevent large holes being produced in the graphene sheets[29]. This in-plane shrinkage is consistent with the loss of bend contours that was observed in low-magnification TEM images during *in-situ* ion irradiation (Fig. 1 and supplementary information Fig. S1). Modelling of these types of topological defect using density functional theory has suggested that they are associated with a localised buckling of the graphene sheet[45–47]. This is expected to produce the streaking of the diffraction patterns of single-layer graphene observed for He ion irradiation fluences of $\sim 10^{16}$ ions cm^{-2} (Fig. 2d–g) and the start of stage 2 in the Raman spectra (Fig. 3a) where the local bonding begins to change from sp^2 to sp^3 configurations[37].

Quantitative analysis of the defect density using high-resolution STEM imaging was impossible due to the increased level of contamination observed for all samples after ion irradiation (Fig. 5, Fig. 6, and supplementary videos S1 and S2). The origin of the increased contamination in the irradiated case is unclear but it is known that the defective material acts as an energetically favourable site for attracting atoms or molecules onto graphene[49–51]. Fig. 5 shows low magnification HAADF STEM images of irradiated graphene. Electron energy loss spectroscopy measurements suggest that this contamination (brighter white/grey regions in Fig. 5) consists of mainly hydrocarbons with silicon and metal impurities (all are known to be frequently present in these materials from the graphene TEM sample preparation[21,52]). With increased fluence, the level of contamination was found to increase and the clean areas of graphene (dark areas visible in Fig. 5) became smaller. The observation of the increased contamination further suggests that the surface contamination may account for the higher estimated topological defect densities found via Raman spectra (Fig. 3) compared to those observed in atomic resolution images.

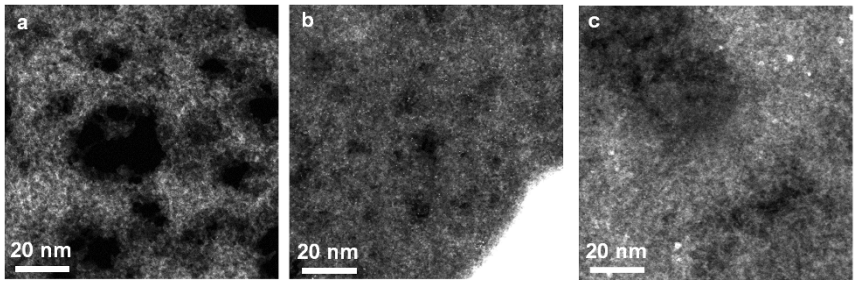

Figure 5 | Representative overview HAADF images of single-layer graphene samples. After irradiation with 30 keV He to fluences of (a) 3.0×10^{15} ions cm^{-2} (b) 6.0×10^{15} ions cm^{-2} and (c) 9.6×10^{15} ions cm^{-2}.

For the high-resolution imaging conditions used in this work, pristine graphene (Fig. 4a) is found to be stable over several hours of imaging. However, this is not the case for defective graphene as the activation energy for bond rotation is considerably lower (4–10 eV compared to ~18–20 eV for knock-on damage of pristine material[7]). Fig. 6 demonstrates the instability of the topological defects during extended imaging (full videos available in supplementary videos S1–S2). Fig. 6a illustrates a 90° bond rotation for the adjoined heptagons in a Stone-Thrower-Wales defect that occurred over ~7 seconds of imaging. However, other highly defective regions were more stable, demonstrating only limited reconstruction after ~30 seconds of imaging as shown in Fig. 6b.

Conclusion

In conclusion, we have observed *in-situ* the macroscopic shrinkage of graphene sheets produced by 30 keV He or 6 keV Ar ion irradiation. Raman spectroscopy measurements for the irradiated material are consistent with a higher fraction of sp^3 bonding in the irradiated graphene and allow a quantitative estimation of defect density. Atomic resolution imaging of the irradiated material has shown that the irradiation-induced defects consist of many 5–7 pairs. This type of defect is known to be associated with a localised buckling of the structure which is consistent with the streaking observed in diffraction patterns and with the changes observed in the Raman spectra obtained from irradiated material. Our first STEM observation of the atomic structures of these defects in ion irradiated graphene supports previous theoretical predictions regarding ion irradiation induced damage processes[3,4] and will be beneficial towards the goal of tuning electronic and magnetic properties via irradiation-induced modifications of graphene materials[2,6] as well as for the optimisation of graphene processing with focused ion beams. Furthermore, the direct visualisation of the defects and morphological changes leading to amorphisation in a single atomic plane provides valuable fundamental insight into the irradiation induced damage sequence of bulk layered materials such as nuclear graphite and sheet silicate minerals.

Methods

In-situ ion irradiation experiments were performed using the MIAMI *in-situ* ion irradiation TEM facility at the University of Huddersfield, UK. This instrument consists of a JEOL JEM-2000FX TEM modified to allow the sample to be ion irradiated while microstructural changes can be continuously monitored via TEM imaging and diffraction[53]. In the current study 30 keV He or 6 keV Ar ions beams were used at an angle of 30° to the imaging electron beam. The diameter of the ion beam is ~1 mm and care was taken to ensure that the ion beam is coincident with the centre of the TEM grid so that the full field of view is irradiated uniformly. The TEM was operated at 80 kV and with a low current density to reduce the likelihood of knock-on irradiation damage from the electron beam[7]. Selected area electron diffraction patterns were acquired using a selected area aperture with a diameter on the sample of ~1 μm. Suspended graphene TEM samples were prepared by transferring micromechanically cleaved graphene from SiO_2/Si substrate onto Quantifoil TEM grids with perforated carbon films according to the method in Ref. 54. Repeat experiments were performed for differing sample thicknesses and ion flux and the *in-*

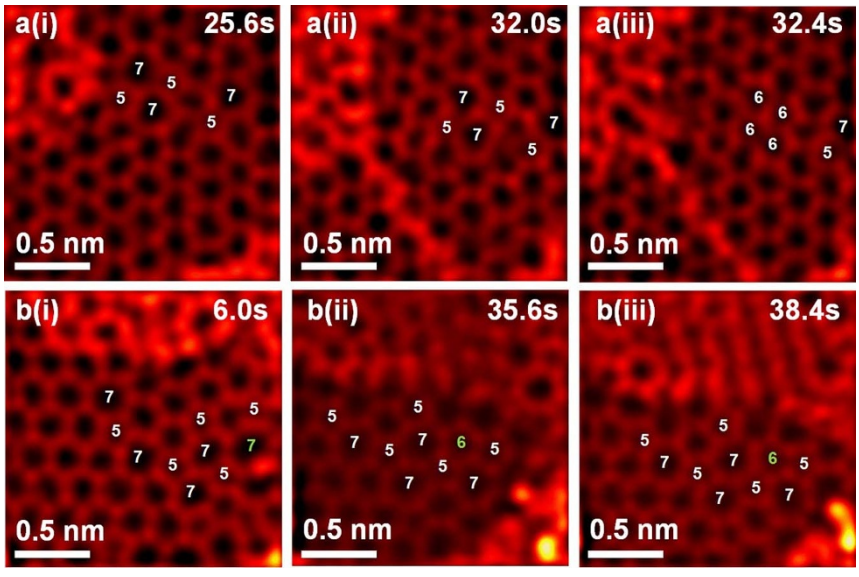

Figure 6 | Structural changes induced in defective graphene due to imaging with a 60 keV electron beam. Sequences of filtered HAADF images a(i–iii) and b(i–iii) showing single-layer graphene that had previously been irradiated *in-situ* using 30 keV He ions to a fluence of 6.0×10^{15} ions cm^{-2} and 9.6×10^{15} ions cm^{-2}, respectively. The time of the image within the complete video sequence is labelled top right (acquisition time was ~0.4 seconds/frame). Image processing routines based on a difference of Gaussians[48] have been used to enhance visibility of defects (raw images are provided in supplementary material Fig. S6 and full videos for (a) and (b) are available in Video S1 and Video S2, respectively).

situ ion irradiation was halted at various ion fluences between 10^{13} and 10^{16} ions cm^{-2} to allow complementary *ex-situ* analysis of defect formation using atomic resolution STEM imaging and Raman spectroscopy. *Ex-situ* Raman measurements were performed using a Renishaw 1000 Raman system with a laser of 514 nm and a ~2 μm spot size. The laser power was limited to ~0.25 mW to avoid sample heating. Raman spectra from identical regions before and after ion irradiation have been compared in order to confirm the expected ion fluence and likely defect density. Atomic resolution STEM imaging was achieved using an aberration corrected Nion UltraSTEM100 with a probe size of 1.1 Å and a beam current of ~45 pA. The instrument was operated at an accelerating voltage of 60 kV in order to reduce the likelihood of knock-on damage even in defective single-layer graphene and the near-ultra-high vacuum of the microscope (less than 5×10^{-9} Torr at the sample) also contributed to reducing the likelihood of contamination.

1. Novoselov, K. S. *et al.* A roadmap for graphene. *Nature* **490**, 192–200 (2012).
2. Chen, J.-H., Cullen, W., Jang, C., Fuhrer, M. & Williams, E. Defect Scattering in Graphene. *Phys. Rev. Lett.* **102**, 236805 (2009).
3. Lehtinen, O., Kotakoski, J., Krasheninnikov, A. V. & Keinonen, J. Cutting and controlled modification of graphene with ion beams. *Nanotechnology* **22**, 175306 (2011).
4. Lehtinen, O. *et al.* Effects of ion bombardment on a two-dimensional target: Atomistic simulations of graphene irradiation. *Phys.Rev. B* **81**, 153401 (2010).
5. Lahiri, J., Lin, Y., Bozkurt, P., Oleynik, I. I. & Batzill, M. An extended defect in graphene as a metallic wire. *Nat. Nano.* **5**, 326–329 (2010).
6. Nair, R. R. *et al.* Spin-half paramagnetism in graphene induced by point defects. *Nat Phys* **8**, 199–202 (2012).
7. Kotakoski, J., Krasheninnikov, A. V., Kaiser, U. & Meyer, J. C. From Point Defects in Graphene to Two-Dimensional Amorphous Carbon. *Phys. Rev. Lett.* **106**, 105505 (2011).
8. Warner, J. H. *et al.* Dislocation-Driven Deformations in Graphene. *Science* **337**, 209–212 (2012).
9. Huang, P. Y. *et al.* Grains and grain boundaries in single-layer graphene atomic patchwork quilts. *Nature* **469**, 389–392 (2011).
10. Meyer, J. C. *et al.* Direct Imaging of Lattice Atoms and Topological Defects in Graphene Membranes. *Nano Lett.* **8**, 3582–3586 (2008).
11. Girit, C. O. *et al.* Graphene at the Edge: Stability and Dynamics. *Science* **323**, 1705–1708 (2009).
12. Russo, C. J. & Golovchenko, J. A. Atom-by-atom nucleation and growth of graphene nanopores. *Proc. Natl. Acad. Sci.* **109**, 5953–5957 DOI:10.1073/pnas.1119827109 (2012).
13. Wang, H. *et al.* Doping Monolayer Graphene with Single Atom Substitutions. *Nano Letters* **12**, 141–144 (2012).
14. Lehtinen, O. *et al.* Non-invasive transmission electron microscopy of vacancy defects in graphene produced by ion irradiation. *Nanoscale* **6**, 6569 (2014).
15. Angelova, P. *et al.* A Universal Scheme to Convert Aromatic Molecular Monolayers into Functional Carbon Nanomembranes. *ACS Nano* **7**, 6489–6497 (2013).
16. Eder, F. R., Kotakoski, J., Kaiser, U. & Meyer, J. C. A journey from order to disorder — Atom by atom transformation from graphene to a 2D carbon glass. *Sci. Rep.* **4**, 4060; DOI:10.1038/srep04060 (2014).
17. Ramasse, Q. M. *et al.* Probing the Bonding and Electronic Structure of Single Atom Dopants in Graphene with Electron Energy Loss Spectroscopy. *Nano Lett.* **13**, 4989–4995 (2013).
18. Suenaga, K. & Koshino, M. Atom-by-atom spectroscopy at graphene edge. *Nature* **468**, 1088–1090 (2010).
19. Nicholls, R. J. *et al.* Probing the Bonding in Nitrogen-Doped Graphene Using Electron Energy Loss Spectroscopy. *ACS Nano* **7**, 7145–7150 (2013).
20. Bangert, U. *et al.* Ion Implantation of Graphene—Toward IC Compatible Technologies. *Nano Lett.* **13**, 4902–4907 (2013).
21. Ramasse, Q. M. *et al.* Direct Experimental Evidence of Metal-Mediated Etching of Suspended Graphene. *ACS Nano* **6**, 4063–4071 (2012).
22. Zan, R., Bangert, U., Ramasse, Q. & Novoselov, K. S. Interaction of Metals with Suspended Graphene Observed by Transmission Electron Microscopy. *J. Phys. Chem. Lett.* **3**, 953–958 (2012).
23. Pan, C. T. *et al.* Nanoscale electron diffraction and plasmon spectroscopy of single- and few-layer boron nitride. *Phys. Rev. B* **85**, 045440 (2012).
24. Zhou, W. *et al.* Single Atom Microscopy. *Microsc. Microanal.* **18**, 1342–1354 (2012).
25. Hashimoto, A., Suenaga, K., Gloter, A., Urita, K. & Iijima, S. Direct evidence for atomic defects in graphene layers. *Nature* **430**, 870–873 (2004).
26. Meyer, J. C. *et al.* Accurate Measurement of Electron Beam Induced Displacement Cross Sections for Single-Layer Graphene. *Phys Rev Lett* **108**, 196102 (2012).
27. Ni, Z. H. *et al.* Graphene Thickness Determination Using Reflection and Contrast Spectroscopy. *Nano Lett.* **7**, 2758–2763 (2007).
28. Williams, D. B. & Carter, C. B. *Transmission Electron Microscopy, Part3: Imaging, Chapter 24. Second edn*, (Springer, 2009).
29. Jeong, B., Ihm, J. & Lee, G.-D. Stability of dislocation defect with two pentagon-heptagon pairs in graphene. *Phys.Rev.B* **78**, 165403 (2008).
30. Heggie, M. I., Suarez-Martinez, I., Davidson, C. & Haffenden, G. Buckle, ruck and tuck: A proposed new model for the response of graphite to neutron irradiation. *J. Nucl. Mater* **413**, 150–155 (2011).
31. Karthik, C., Kane, J., Butt, D. P., Windes, W. E. & Ubic, R. In situ transmission electron microscopy of electron-beam induced damage process in nuclear grade graphite. *J. Nucl. Mater* **412**, 321–326 (2011).
32. Tsai, S.-C., Huang, E. W., Kai, J.-J. & Chen, F.-R. Microstructural evolution of nuclear grade graphite induced by ion irradiation at high temperature environment. *J. Nucl.Mater* **434**, 17–23 (2013).
33. Hinks, J. A. *et al.* Dynamic microstructural evolution of graphite under displacing irradiation. *Carbon* **68**, 273–284 (2014).
34. Ziegler, J. F., Ziegler, M. D. & Biersack, J. P. SRIM – The stopping and range of ions in matter (2010). *Nucl. Instrum. Methods Phys. Res. Sect. B* **268**, 1818–1823 (2010).
35. Meyer, J. C. *et al.* On the roughness of single- and bi-layer graphene membranes. *Solid State Comm.* **143**, 101–109 (2007).
36. Henrard, L., Loiseau, A., Journet, C. & Bernier, P. Study of the symmetry of single-wall nanotubes by electron diffraction. *Eur. Phys. J. B* **13**, 661–669 (2000).
37. Ferrari, A. C. & Robertson, J. Interpretation of Raman spectra of disordered and amorphous carbon. *Phys. Rev. B* **61**, 14095–14107 (2000).
38. Ferrari, A. C. Raman spectroscopy of graphene and graphite: Disorder, electron–phonon coupling, doping and nonadiabatic effects. *Solid State Comm.* **143**, 47–57 (2007).
39. Lucchese, M. M. *et al.* Quantifying ion-induced defects and Raman relaxation length in graphene. *Carbon* **48**, 1592–1597 (2010).
40. Iqbal, M. W., Singh, A. K., Iqbal, M. Z. & Eom, J. Raman fingerprint of doping due to metal adsorbates on graphene. *J.Phys. Cond. Mat.* **24**, 335301 (2012).
41. Cançado, L. G. *et al.* Quantifying Defects in Graphene via Raman Spectroscopy at Different Excitation Energies. *Nano Lett.* **11**, 3190–3196 (2011).
42. Compagnini, G., Giannazzo, F., Sonde, S., Raineri, V. & Rimini, E. Ion irradiation and defect formation in single layer graphene. *Carbon* **47**, 3201–3207 (2009).
43. Eckmann, A. *et al.* Probing the Nature of Defects in Graphene by Raman Spectroscopy. *Nano Lett.* **12**, 3925–3930 (2012).
44. Casiraghi, C. Doping dependence of the Raman peaks intensity of graphene close to the Dirac point. *Phys. Rev. B* **80**, 233407 (2009).
45. Yazyev, O. V. & Louie, S. G. Topological defects in graphene: Dislocations and grain boundaries. *Phys. Rev. B* **81**, 195420 (2010).
46. Lusk, M. & Carr, L. Nanoengineering Defect Structures on Graphene. *Phys. Rev. Lett.* **100**, 175503 (2008).
47. Ma, J., Alfè, D., Michaelides, A. & Wang, E. Stone-Wales defects in graphene and other planar sp^2-bonded materials. *Phys.Rev.B* **80**, 033407 (2009).
48. Krivanek, O. L. *et al.* Low Voltage Electron Microscopy: Principles and Applications. *Chapter 6: Gentle STEM of Single Atoms: Low keV Imaging and Analysis at Ultimate Detection Limits*. Bell, D. C. & Erdman, N. (eds.). 119–163, First edn, (John Wiley & Sons, Ltd, 2013).
49. Medina, H., Lin, Y.-C., Obergfell, D. & Chiu, P.-W. Tuning of Charge Densities in Graphene by Molecule Doping. *Adv. Funct. Mater.* **21**, 2687–2692 (2011).
50. Boukhvalov, D. W. & Katsnelson, M. I. Chemical Functionalization of Graphene with Defects. *Nano Lett.* **8**, 4373–4379 (2008).
51. Chen, L. *et al.* Atomic chemisorption on graphene with Stone–Thrower–Wales defects. *Carbon* **49**, 3356–3361 (2011).
52. Gass, M. H. *et al.* Free-standing graphene at atomic resolution. *Nature Nano.* **3**, 676–681 (2008).
53. Hinks, J. A., van den Berg, J. A. & Donnelly, S. E. MIAMI: Microscope and ion accelerator for materials investigations. *J. Vac. Sci. Technol A* **29**, 021003 (2011).
54. Meyer, J. C., Girit, C. O., Crommie, M. F. & Zettl, A. Imaging and dynamics of light atoms and molecules on graphene. *Nature* **454**, 319–322 (2008).

Acknowledgments

The authors would like to acknowledge Professor Sir Andre K. Geim for the experimental support of graphene sample fabrication. We thank Dr. Libo Deng and Dr. Cinzia Casiraghi for the informative comments on Raman measurements and Narayanannamboothiri Jayaram for the useful discussions of TEM specimen preparations. The SuperSTEM Laboratory is funded by the U.K. Engineering and Physical Sciences Research Council (EPSRC). We thank the EPSRC for funding under grant numbers EP/I003223/1, EP/G035954/1 and EP/K016946/1 and the Defense Threat Reduction Agency (USA) under grant number HDTRA-1-12-0013.

Author contributions

S.J.H. and S.E.D. conceived the experiments. C.-T.P. prepared the samples. C.-T.P., J.A.H., S.J.H., G.G. and Q.M.R. performed the experiments. C.-T.P., J.A.H. and S.J.H. wrote the manuscript. All authors contributed to interpreting the results and commented on the manuscript.

Additional information

Supplementary information accompanies this paper at http://www.nature.com/scientificreports

Competing financial interests: The authors declare no competing financial interests.

How to cite this article: Pan, C.-T. *et al.* In-situ observation and atomic resolution imaging of the ion irradiation induced amorphisation of graphene. *Sci. Rep.* **4**, 6334; DOI:10.1038/srep06334 (2014).